High-Speed Data Access with Enhanced Interference Suppression over Wideband CDMA Networks*

Sofiène AFFES[1], Karim CHEIKHROUHOU[2], and Paul MERMELSTEIN[1]
1: INRS-Télécommunications, Université du Québec
800, de la Gauchetière Ouest, Suite 6900, Montréal, Québec, H5A 1K6, Canada
2: École Nationale d'Ingénieurs de Tunis
BP 37, Le Belvédère , Tunis, 1002, Tunisia
{affes,cheikhro,mermel}@inrs-telecom.uquebec.ca

Abstract— **Recently we developed an efficient multiuser upgrade of the single-user spatio-temporal array-receiver (STAR), referred to as interference subspace rejection (ISR). The resulting STAR-ISR receiver offers a number of implementation modes covering a large range in performance and complexity for wideband CDMA networks. Here we apply STAR-ISR to high data-rate (HDR) transmissions by extending operation to delay spreads larger than the symbol duration. Low processing gain situations render symbol timing extremely difficult, especially with RAKE-type receivers. For HDR links of 512 Kbps in 5 MHz bandwidth, simulations indicate that the simplest mode of STAR-ISR outperforms the 2D-RAKE-PIC by factor 4 to 5 in spectrum efficiency while requiring the same order of complexity. This gain increases up to factor 7.5 in high Doppler.**

I. Introduction

We have recently proposed a unifying framework for a new class of receivers that employ linearly-constrained interference cancellation for multiuser detection in wideband CDMA [1]. These detectors referred to as ISR operate in multiple mixed-traffic scenarios and in various modes, ranging in performance and complexity from linear receivers to interference cancellers. In addition to interference rejection, they perform space and time diversity combining, array processing and synchronization using STAR [2],[3].

So far, however, we investigated the STAR-ISR receiver solutions with delay spreads smaller in chips than the processing gain. HDR applications require spreading factors smaller than the delay spread. These low processing gain situations render symbol timing extremely difficult. More importantly, they see inter-symbol interference (ISI) and inter-path interference (IPI) increase dramatically to the point of seriously deteriorating the receiver performance. From 3G wideband radio-channel models [4],[5],[6], we made an assessment that current synchronization techniques cannot achieve satisfactory performance with processing gains below 32 (see high-rate example in [2]). A review of the recent literature on synchronization in wideband CDMA receivers confirms this limitation. The proposed HSDPA standard [7] exemplifies this limit. The 32 minimum spreading factor limit there sets a bound on the peak rate achievable with BPSK. It hence suggests use of higher-order modulations to increase the peak rate up to 540 Kbps per spreading code with 64-QAM.

Similarly, we are investigating use of higher-order modulations [8]. However, increase in the transmission rate with more power-efficient lower-order modulations such as BPSK or QPSK offers an even more promising path for achieving substantial gains both in peak rate and spectrum efficiency. Accordingly, we propose a HDR implementation that operates STAR-ISR at processing gains lower than 32.

The HSDPA standard considers implementation of PIC, but leaves open all issues related to synchronization and channel identification [7]. Yet despite reports on the challenging problems met when operating RAKE-type receivers in HDR applications [7],[9], the 2D-RAKE-PIC is currently accepted as the best receiver candidate for implementation to our knowledge [9]-[12]. In this work, we develop an enhanced HDR implementation of the 2D-RAKE-PIC as a reference. For HDR links of 512 Kbps in 5 MHz bandwidth, simulations indicate that the simplest mode of STAR-ISR outperforms the 2D-RAKE-PIC by factor 4 to 7.5 in spectrum efficiency while requiring the same complexity.

II. Data Model and Formulation of the Problem

We consider the uplink of an asynchronous cellular CDMA system where each base-station is equipped with a receiving antenna-array of M sensors. Application to the downlink will be studied in a future work. For the sake of simplicity, we assume that all desired users in the served cell or sector, NI in number, transmit with the same BPSK modulation and at the same rate $1/T$, where T is the symbol duration. This corresponds to the homogeneous traffic scenario treated in [1]. Extension to the mixed-rate traffic situation with mixed symbol modulations and/or rates is *ad hoc*. The BPSK[1] sequence $b^i(t)$ of a desired user with index $i \in \{1, \ldots, NI\}$ is spread by a personal PN code $c^i(t)$ at a rate $1/T_c$, where T_c is the chip pulse duration. The processing gain is given by $L = T/T_c$. We assume the use of long codes. We write the spreading-code segment over the n-th period T as:

$$c_n^i(t) = \sum_{l=0}^{L-1} c_{n,l}^i \phi(t - lT_c - nT) \,, \qquad (1)$$

where $c_{n,l}^i = \pm 1$ for $l = 0, \ldots, L-1$, is a random sequence of length L and $\phi(t)$ is the chip pulse. Finally, we assume a multipath Rayleigh fading environment with P resolvable

* Work supported by the Bell/Nortel/NSERC Industrial Research Chair in Personal Communications and by the NSERC Research Grants Program.

[1]We assume use of pilot symbols with a very small overhead and hence implement coherent detection with the coherent channel identification technique developed in [13].

paths with a delay spread $\Delta\tau$. $N_f = MP$ hence denotes the total number of diversity fingers.

In contrast to [1],[2],[3], here we no longer require that the delay spread be small compared to the symbol duration (*i.e.*, $\Delta\tau \ll T$), a very limiting assumption indeed in the HDR case where very likely $\Delta\tau > T$. Similarly to [2], we define the enlarged delay-spread $\overline{\Delta\tau} > \Delta\tau$ to allow an increased uncertainty margin (*i.e.*, $T < \Delta\tau < \overline{\Delta\tau}$) for the tracking of time-varying multipaths due to clock drifts and receiver mobility. We also define $L_{\overline{\Delta}} = \lceil \overline{\Delta\tau}/T_c \rceil$ and $Q_{\overline{\Delta}} = \lceil \overline{\Delta\tau}/T \rceil$ the corresponding lengths in chip samples and symbols, respectively.

Similarly to [1], we assume that the channel parameters (*i.e.*, delays, powers, fade magnitudes and phases) vary slowly and neglect their variation over Q symbol durations (*i.e.*, QT). This allows for data processing in successive blocks of Q symbols. Hence, after chip-pulse matched-filtering, sampling at the chip rate and framing over $QL + L_{\overline{\Delta}}$ chip samples at the processing rate $1/T_P$ where $T_P = QT$ denotes the block processing period, we obtain the $M \times (QL + L_{\overline{\Delta}})$ matched-filtering observation matrix for the n-th block (see details in [1]):

$$\mathbf{Y}_n = [Y_n(0), Y_n(T_c), \ldots, Y_n((QL + L_{\overline{\Delta}} - 1)T_c)] \ . \quad (2)$$

Defining for convenience of notation a vector $\underline{Y}$ as a matrix $\mathbf{Y}$ reshaped column-wise, we rewrite the vectorized matched-filtering observation matrix $\mathbf{Y}_n$ of Eq. (2) with respect to the k-th symbol ($k = 0, \ldots, Q-1$) of the i-th desired user ($i = 1, \ldots, NI$) as:

$$\begin{aligned} \underline{Y}_n &= \psi_n^i b_{nQ+k}^i \underline{Y}_{k,n}^i + \left\{ \psi_n^i \underline{I}_{\mathrm{ISI},n}^{i,k} + \sum_{\substack{i'=1 \\ i' \neq i}}^{NI} \psi_n^{i'} \underline{Y}_n^{i'} \right\} + \underline{N}_n \\ &= s_n^{i,k} \underline{Y}_{k,n}^i + \underline{I}_n^{i,k} + \underline{N}_n \ , \end{aligned} \quad (3)$$

where for the i-th user at the n-th data block $b_{nQ+k}^i = b^i((nQ+k)T)$, $s_n^{i,k} = \psi_n^i b_{nQ+k}^i$ is the k-th signal component, $\underline{Y}_{k,n}^i$ is the canonic user-observation vector of the k-th symbol, $\underline{Y}_n^i$ is the user-observation vector and $\underline{I}_{\mathrm{ISI},n}^{i,k} = \underline{Y}_n^i - b_{nQ+k}^i \underline{Y}_{k,n}^i$ is the ISI vector over the the k-th symbol [1]. $\underline{I}_n^{i,k}$, referred to as the interference vector in the following, denotes the part of the multiple access interference (MAI) vector to be suppressed, including ISI from user i over its k-th symbol. The noise vector $\underline{N}_n$ comprises the rest of the MAI from all other users in the system and the preprocessed thermal noise [1].

Provided that the data block edges are properly positioned after time acquisition[2] (see Fig. 1), the parametric data decompositions introduced in [1] detail the structure of the interference vector as follows:

$$\underline{I}_n^{i,k} = \sum_{i'=1}^{NI} \sum_{f=1}^{N_f} \sum_{k'=-Q_{\overline{\Delta}}}^{Q+Q_{\overline{\Delta}}-1} \psi_n^{i'} \zeta_{f,n}^{i'} b_{nQ+k}^{i'} \underline{Y}_{k',n}^{i',f} \bar{\delta}_{i',i}^{k',k} \ , \quad (4)$$

[2]We make this assumption in this paper leaving only tracking necessary for permanent update of the time-delays within the enlarged delay-spread $\overline{\Delta\tau} > \Delta\tau$.

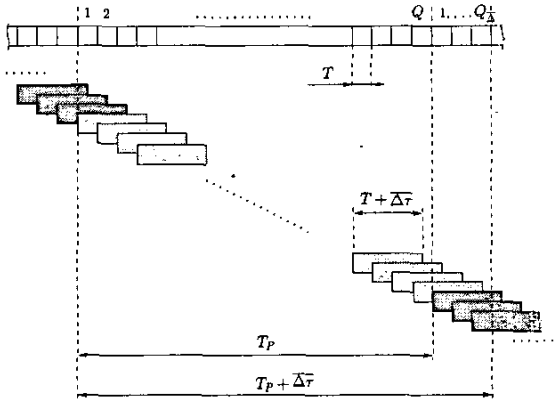

Fig. 1. Signal structure of the data block: Each symbol is "spread" by multipath propagation within a temporal cluster of duration $T + \overline{\Delta\tau}$. Each symbol-cluster is represented by a rectangle. The Q light-shaded clusters correspond to the desired symbols to be extracted in the current data block while the $2Q_{\overline{\Delta}}$ dark-shaded ones correspond to interference (*i.e.*, edge effect).

where finger $f = (p-1)M + m \in \{1, \ldots, N_f\}$, denotes antenna $m \in \{1, \ldots, M\}$ and propagation path $p \in \{1, \ldots, P\}$, $\zeta_{f,n}^u$ stands for the corresponding propagation coefficient, $\underline{Y}_{k,n}^{u,f}$ is the canonic diversity-observation vector [1], and $\bar{\delta}_{i',i}^{k',k} = 0$ if $i' = i$ and $k' = k$, and 1 otherwise.

In Eq. (4), note that summation over the symbol index k' ranges from $-Q_{\overline{\Delta}}$ to $Q + Q_{\overline{\Delta}} - 1$ instead of -1 to Q in [1]. There we considered the case of a delay spread smaller than the symbol duration leading to $Q_{\overline{\Delta}} = 1$. As shown in Fig. 1, the data block of duration $T + \overline{\Delta\tau}$ includes all the desired signal contribution from the Q symbols to be extracted, assigned index k' from 0 to $Q-1$. However, the signal structure of the data block accounts for contribution from adjacent blocks, namely $Q_{\overline{\Delta}}$ past symbols assigned index k' from $-Q_{\overline{\Delta}}$ to -1 as well as $Q_{\overline{\Delta}}$ future symbols assigned index k' from Q to $Q + Q_{\overline{\Delta}} - 1$. The resulting parametric decompositions of interference in Eq. (4) for large delay-spread situations give rise to the following HDR implementation of STAR-ISR.

III. HDR Implementation of STAR-ISR

A. HDR Symbol Estimation with ISR

Using joint ISR detection [1], we extract the k-th symbol ($k = 0, \ldots, Q-1$) of the i-th desired user ($i = 1, \ldots, NI$) with the following combiner:

$$\underline{W}_n^{i,k} = \frac{\mathbf{\Pi}_n^{i,k} \hat{\underline{Y}}_{k,n}^i}{\hat{\underline{Y}}_{k,n}^{i\,H} \mathbf{\Pi}_n^{i,k} \hat{\underline{Y}}_{k,n}^i} = \mathbf{\Pi}_n^{i,k} \frac{\hat{\underline{Y}}_{k,n}^i}{\|\hat{\underline{Y}}_{k,n}^i\|^2} = \mathbf{\Pi}_n^{i,k} \underline{W}_{\mathrm{MRC},n}^{i,k}, \quad (5)$$

where:

$$\mathbf{\Pi}_n^{i,k} = \mathbf{I}_{N_T} - \hat{\mathbf{C}}_n \mathbf{Q}_n \hat{\mathbf{C}}_n^{i,k\,H} \ , \quad (6)$$

is a projection orthogonal to the interference vector $\underline{I}_n^{i,k}$ in the observation space of dimension $N_T = M(QL + L_{\overline{\Delta}})$.

ISR Mode	$\hat{\mathbf{C}}_n^{i,k} = \left[\ldots, \hat{\mathbf{C}}_{j,n}^{i,k}, \ldots\right]$
TR	$\left[\sum_{i'=1}^{NI}\sum_{f=1}^{N_f}\sum_{k'=-Q_{\overline{\Delta}}}^{Q+Q_{\overline{\Delta}}-1} \hat{\psi}_n^{i'}\hat{\zeta}_{f,n}^{i'}\hat{b}_{nQ+k}^{i'}\hat{\underline{Y}}_{k',n}^{i',f}\bar{\delta}_{i',i}^{k',k}\right]$ $\Rightarrow N_c = 1$
R	$\left[\ldots, \sum_{f=1}^{N_f}\sum_{k'=-Q_{\overline{\Delta}}}^{Q+Q_{\overline{\Delta}}-1} \hat{\zeta}_{f,n}^{i'}\hat{b}_{nQ+k}^{i'}\hat{\underline{Y}}_{k',n}^{i',f}\bar{\delta}_{i',i}^{k',k}, \ldots\right]$ $\Rightarrow N_c = NI$
D	$\left[\ldots, \sum_{k'=-Q_{\overline{\Delta}}}^{Q+Q_{\overline{\Delta}}-1} \hat{b}_{nQ+k}^{i'}\hat{\underline{Y}}_{k',n}^{i',f}\bar{\delta}_{i',i}^{k',k}, \ldots\right]$ $\Rightarrow N_c = N_f NI$
H	$\left[\ldots, \sum_{f=1}^{N_f} \hat{\zeta}_{f,n}^{i'}\hat{\underline{Y}}_{k',n}^{i',f}\bar{\delta}_{i',i}^{k',k}, \ldots\right]$ $\Rightarrow N_c = (Q+2Q_{\overline{\Delta}})NI$

Tab. 1. The signal blocking matrix $\hat{\mathbf{C}}_n^{i,k}$ and the corresponding number of constraints or columns N_c for each ISR mode. Each generic column $\hat{\mathbf{C}}_{j,n}^{i,k}$ shown above is divided by the norm of the corresponding generic column $\hat{\mathbf{C}}_{j,n}$ of the constraint matrix $\hat{\mathbf{C}}_n$ (obtained here by replacing $\bar{\delta}_{i',i}^{k',k}$ with 1).

$\hat{\mathbf{C}}_n$ and $\hat{\mathbf{C}}_n^{i,k}$ denote the constraint matrix and the corresponding signal blocking matrix, respectively [1].

In Tab. 1 we show how to form these matrices for different ISR modes, which decompose or regroup interference vectors from different interference subspace characterizations [1]. It is in the constraint matrices of Tab. 1 that we observe the modifications required for large delay-spreads in HDR applications. Indeed in the DF (decision feedback) modes, construction of the constraint matrices requires now estimation of $Q_{\overline{\Delta}}$ past symbols from the previous data block (with ISR combining) as well as estimation of $Q_{\overline{\Delta}}$ future symbols from the next data block (with simple MRC) [1]. To complete construction of the constraint matrices, the Q target symbols in the current data block are estimated in an initial stage with MRC (*i.e.*, stage 0) [1]. Once the constraint matrices are available, the target symbols are reestimated with ISR combining. This process is repeated iteratively in a multistage structure and terminated say after N_s stages [1]. In the H mode, however, neither decision feedback nor processing delays are required. But in contrast to the DF modes, the number of constraints N_c increases from $(Q+2)NI$ for small delay spreads [1] to $(Q+2Q_{\overline{\Delta}})NI$ in Tab. 1.

ISR combining in Eq. (5) is actually implemented in cascade, first by projection of the matched-filtering observation vector to yield the new observation:

$$\underline{Y}_{\Pi,n}^{i,k} = \mathbf{\Pi}_n^{i,k}\underline{Y}_n \ , \tag{7}$$

then by coherent MRC combining to estimate the k-th signal component of the i-th user as follows:

$$\hat{s}_n^{i,k} = \text{Real}\left\{\underline{W}_{\text{MRC},n}^{i,k^H}\underline{Y}_{\Pi,n}^{i,k}\right\} \ . \tag{8}$$

Taking the sign of the signal components above allows estimation of the BPSK symbols $\hat{b}_{nQ+k}^i$ for $k = 0, \ldots, Q-1$ and for $i = 1, \ldots, NI$.

B. HDR Channel Identification with STAR

Note that the new observation $\underline{Y}_{\Pi,n}^{i,k}$ is almost interference-free (in the sense that any contribution from the interference vector $\underline{I}_n^{i,k}$ is rejected). By despreading its matrix-reshaped form $\mathbf{Y}_{\Pi,n}^{i,k}$, defined as

$$\mathbf{Y}_{\Pi,n}^{i,k} = \left[Y_{\Pi,n}^{i,k}(0), \ldots, Y_{\Pi,n}^{i,k}((QL+L_{\overline{\Delta}}-1)T_c)\right] \ , \tag{9}$$

with the code segment that spreads the k-th symbol of the i-th user, we obtain the following $M \times L_{\overline{\Delta}}$ reduced-size postcorrelation matrix [2]:

$$\mathbf{Z}_{\Pi,n}^{i,k} = \left[Z_{\Pi,n}^{i,k}(0), \ldots, Z_{\Pi,n}^{i,k}((L_{\overline{\Delta}}-1)T_c)\right] \ , \tag{10}$$

where for $l = 0, \ldots, L_{\overline{\Delta}}-1$:

$$Z_{\Pi,n}^{i,k}(lT_c) = \frac{1}{L}\sum_{l'=0}^{L-1} Y_n((kL+l+l')T_c)c_{nQ+k,l'}^i \ . \tag{11}$$

The resulting vector-reshaped postcorrelation vector is also almost interference-free and has the following structure [14]:

$$\underline{Z}_{\Pi,n}^{i,k} \simeq s_n^{i,k}\underline{H}_n^i + \underline{N}_{\text{PCM},n}^{i,k} \ , \tag{12}$$

where $\underline{H}_n^i$ denotes the $ML_{\overline{\Delta}} \times 1$ spatio-temporal propagation vector of the i-th user [1],[2],[3] and $\underline{N}_{\text{PCM},n}^{i,k}$ is the postcorrelation noise vector obtained by projection and despreading of the spatio-temporal noise vector $\underline{N}_n$ of Eq. (3).

The expression for the new postcorrelation vector $\underline{Z}_{\Pi,n}^{i,k}$ in Eq. (12) approaches that of a single-user observation if $\underline{N}_{\text{PCM},n}^{i,k}$ is approximated as an uncorrelated spatio-temporal noise vector. It allows implementation of STAR in a single-user structure by exploiting the advantages of ISR in the so-called decision feedback identification procedure (DFI) [3] with projection (Π-DFI) proposed in [14]. In more adverse near-far situations, the Π-DFI procedure guarantees more reliable channel identification than simple DFI [3] and increases the near-far resistance of STAR-ISR [14]. This solution was however investigated in [14] in the case of a small delay-spread without use of a block processing structure (*i.e.*, $Q = 1$). We adapt it below to HDR applications.

We exploit the fact that the channel parameters are assumed constant over the processing period T_P (as reflected in Eq. (12) where the channel $\underline{H}_n^i$ is indeed identical for

Calculation of $\hat{\underline{Y}}^i_{k,n}$	$\frac{1}{n_{\rm CR}}(MLL_{\overline{\Delta}}NIQ)$
Reconstruction of $\hat{\underline{C}}_n$	$M\{2L^2_{\overline{\Delta}}/(QL)+L\}Q\ NI\ N_s$
Projection $\underline{\Pi}^{i,k}_n$	$2M(L+L_{\overline{\Delta}})Q\ NI\ N_s$
Estimation of $\hat{s}^{i,k}_n$	$3M(L+L_{\overline{\Delta}})Q\ NI\ N_s$
Channel identification	$\frac{1}{n_{\rm ID}}(2ML_{\overline{\Delta}}+ML_{\overline{\Delta}}L)NIQ$
Multipath tracking	$\frac{1}{n_{\rm ID}}\{2PL_{\overline{\Delta}}\log_2(L_{\overline{\Delta}})\}NI$

Tab. 2. Estimated complexity items for STAR-ISR-TR ($n_{\rm CR}=1$ for long codes [2]).

all Q target symbols) to update the estimate of the propagation vector $\hat{\underline{H}}^i_n$ at the processing rate using the following block Π-DFI procedure:

$$\hat{\underline{H}}^i_{n+1}=\hat{\underline{H}}^i_n+\frac{\mu}{Q}\sum_{k=0}^{Q-1}\left(\underline{Z}^{i,k}_{\Pi,n}-\hat{\underline{H}}^i_n\hat{s}^{i,k}_n\right)\hat{s}^{i,k*}_n\ , \qquad (13)$$

where μ denotes the adaptation step-size. This procedure is different from the Π-DFI channel identification technique in [14] in that it averages the gradient over all Q target symbols. Direct application of the Π-DFI procedure would instead update the channel estimate more frequently at the symbol rate with similar complexity. To reduce computations, channel update in the new block Π-DFI procedure of Eq. (13) can be carried out at a pace slower than the processing rate, say once every $n_{\rm ID}$ data blocks, using the reduced channel-update-rate option studied in [2]. Next we assess the complexity of the HDR implementation of STAR-ISR in its simplest ISR mode TR (see Tab. 1) [1].

C. Complexity Assessment of HDR STAR-ISR-TR

We consider here the simplest ISR mode TR for complexity assessment of the STAR-ISR receiver. At the same order of complexity, ISR-TR readily outperforms PIC [1],[8] by significant gains in SNR. Complexity assessments were already made in [1]. However, they did not consider the new HDR implementation of STAR-ISR. Besides, the reference solution we considered there for comparisons was a combination of multistage PIC with STAR. Here we consider instead as a reference a combination of multistage PIC with the enhanced 2D-RAKE version with the early-late gate developed in [2]. Indeed, the 2D-RAKE-PIC is currently accepted as the best receiver candidate for implementation to our knowledge [9]-[12], despite reports on challenging problems met when operating RAKE-type receivers with HDR transmissions [9],[7]. Yet inspired from the HDR implementation of STAR-ISR, we have been able to operate the 2D-RAKE at very low processing gains (see simulations next). More details about our HDR implementation of the 2D-RAKE-PIC will be provided in a future contribution.

In Tab. 2, the computational complexity order of STAR-ISR-TR is itemized in Tab. 2 along its key processing operations. In Fig. 2, however, we plot the complexity per user in Mops (million operations per second) of both STAR-ISR-TR and the 2D-RAKE-PIC versus the processing gain

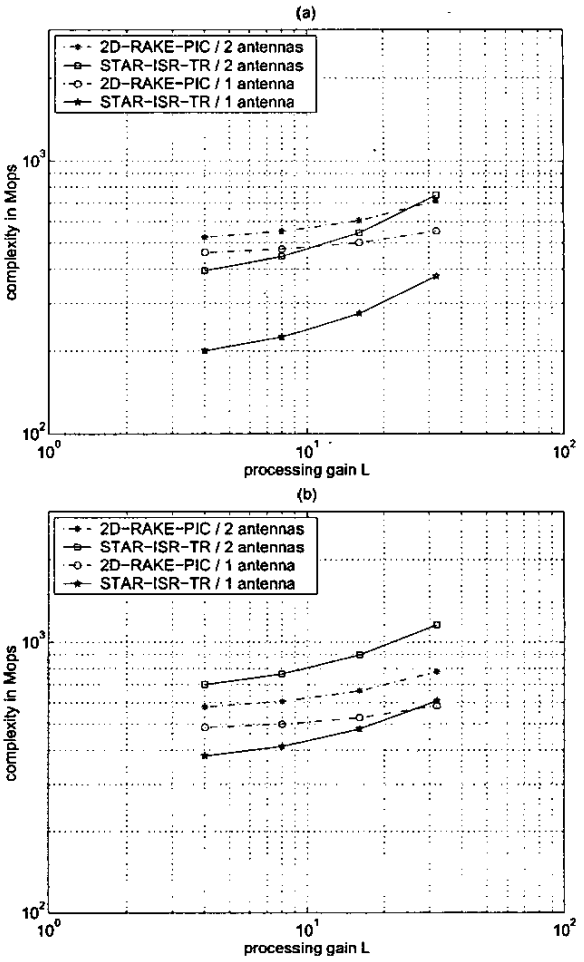

Fig. 2. Complexity per user (at processing rate $1/T_P$ of 64 KHz in 4.096 Mcps) for STAR-ISR-TR and the 2D-RAKE-PIC both with $N_s=1$ stage and $L_{\overline{\Delta}}=32$. (a): slow Doppler (*i.e.*, $n_{\rm ID}=10$), (b): fast Doppler (*i.e.*, $n_{\rm ID}=1$).

L. In the slow Doppler case of Fig. 2-a, STAR-ISR-TR requires less computational complexity than the 2D-RAKE with one or two antennas alike, more so in HDR applications (*i.e.*, low processing gain L). With such transmissions, STAR-ISR-TR with two antennas still requires less computational complexity than the 2D-RAKE with one antenna. In the fast Doppler case of Fig. 2-b, STAR-ISR-TR with one antenna is the least complex. With two antennas, however, it exacts the highest computational cost.

Overall, the orders of complexity for both STAR-ISR-TR and the 2D-RAKE-PIC are in the range of a few hundred Mops, a computational load per user that is in the reach of current digital processors. It should be noted however that complexity figures of the 2D-RAKE-PIC are those for $N_s=1$ stage, therefore optimistic. Simulation results for the 2D-RAKE-PIC will be provided next with $N_s=2$ stages.

Parameter	Value	Comment
R_c	4.096 Mcps	chip rate
R_b	512 Kbps	BPSK bit rate
L	8	spreading factor
Q	8	number of symbols/block
M	2	number of antennas
P	3	number of fading paths
$\bar{\varepsilon}_p^2$	(0, 0, 0) dB	average power profile
f_c	1.9 GHz	carrier frequency
f_D	1.8 Hz	Doppler spread (1 Kmph)
f_{PC}	1600 Hz	PC frequency
ΔP_{PC}	$\pm$ 0.25 dB	PC adjustment
BER_{PC}	10 %	PC BER
$\frac{d\tau}{dt}$	0.046	linear delay drift [ppm]
$\Delta\tau$	8 chips	delay spread
$L_{\widetilde{\Delta}}$	32 chips	enlarged delay-spread
ξ^2	1%	pilot-symbol overhead
γ	0.0	raised cosine rolloff
N_c	16	pulse coefficients
n_{ID}	10	reduced channel ID rate
n_{CR}	1	long codes (see [2])

Tab. 3. Parameters used in the simulations.

IV. Performance Evaluation

We consider a wideband CDMA system with 5 MHz bandwidth and select the setup parameters listed in Tab. 3. We compare the performance of both STAR-ISR-TR and the 2D-RAKE-PIC in terms of required SNR at a BER of 5% before FEC decoding versus the number of users per cell or per sector (*i.e.*, cell or sector load) transmitting at 512 Kbps after channel coding (or for instance 256 Kbps with rate-1/2 channel coding).

In the reference 2D-RAKE-PIC HDR implementation, we use $P_{\max} = 3$ fingers and $n_{\text{RA}} = 2000$ for multipath tracking and reacquisition [2] with the 2D-RAKE and $N_s = 2$ stages with PIC. In a first STAR-ISR-TR HDR implementation, we deactivate the new block Π-DFI procedure and use instead simple DFI (*i.e.*, ISR advantages through projection of the observation before despreading [14] are not exploited). We also use the default ISR structure with $N_s = 1$ stage [1]. This default version is simply referred to as STAR-ISR-TR. In a second implementation referred to as STAR-ISR-TR-M(2), we activate the new block Π-DFI procedure. In a third implementation referred to as STAR-ISR-TR-Π, we implement the multistage option of ISR with $N_s = 2$ stages. In a fourth and last version referred to as STAR-ISR-TR-Π-M(2), we activate both the new block Π-DFI procedure and the multistage option of ISR with $N_s = 2$ stages.

In Fig. 3, we plot with a solid line the required SNR curves versus the number of users for the reference 2D-RAKE-PIC and the four versions of the STAR-ISR-TR HDR implementation explained above. The dashed line gives the load curve for an outcell to incell interference ratio $f_{O/I} = 0.5$ [1]. The 2D-RAKE-PIC cannot accommodate more than 3 users per cell or per sector. On the other hand, STAR-ISR-TR enables the base station to serve 12 simultaneous users per cell or per sector, thereby offering an increase in capacity as high as factor 4. Activation of the new block Π-DFI procedure in STAR-ISR-TR-Π or use of an additional multistage iteration (*i.e.*, $N_s = 2$) in STAR-ISR-TR-M(2) allows accommodation of an additional user up to 13. Curves however indicate that SNR gains obtained with an additional multistage are more significant than those due to the Π-DFI procedure. Combination of both advantages in STAR-ISR-TR-Π-M(2) increases capacity up to 14 simultaneous users per cell or sector, thereby pushing the performance advantage of STAR-ISR-TR over the 2D-RAKE-PIC close to factor 5 in capacity gains.

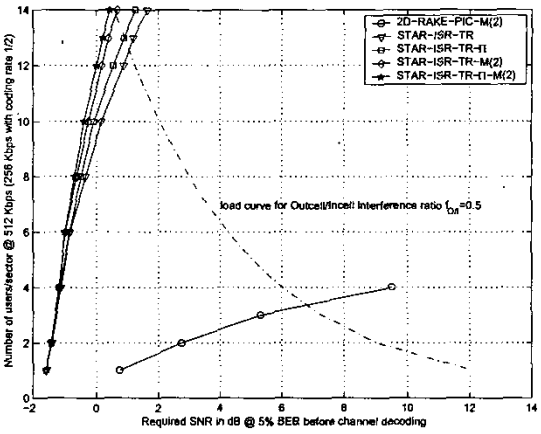

Fig. 3. Required SNR at a BER of 5% before FEC decoding vs. the number of users per cell or sector NI for STAR-ISR-TR and the 2D-RAKE-PIC-M(2) (*i.e.*, $N_s = 2$ stages).

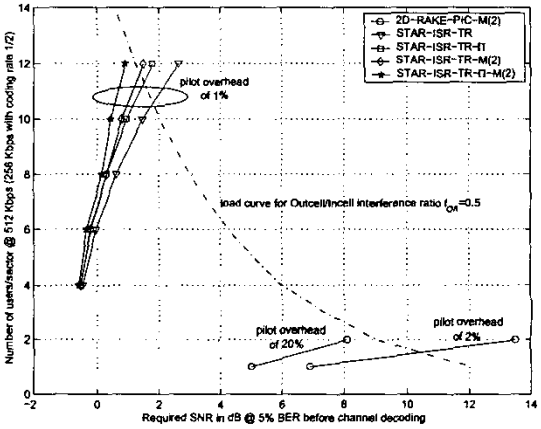

Fig. 4. Same as Fig. 3 with faster channel variations (*i.e.*, Doppler spread of 106 Hz at mobile speed of 60 Kmph and delay drift of 4 ppm, see Tab. IV).

In a second set of simulations, we assess the impact of fast channel variations on performance by increasing the Doppler spread and the delay drift to 106 Hz and 4 ppm, respectively. Hence, we disable the reduced channel-update-rate option [2] (*i.e.*, $n_{\text{ID}} = 1$, see subsection III-B) at the

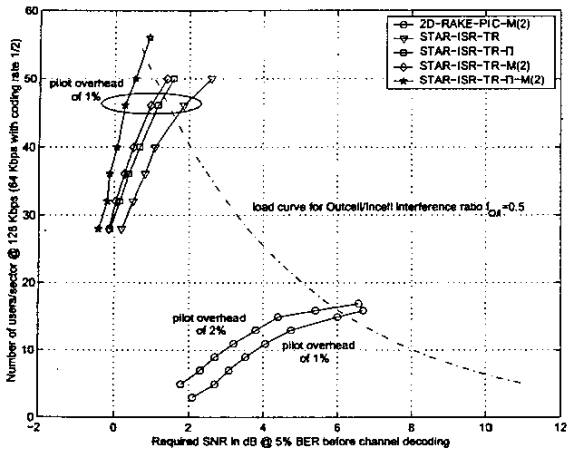

Fig. 5. Same as Fig. 3 with lower data rate (*i.e.*, 128 Kbps at spreading factor of 32, see Tab. IV).

cost of additional complexity (see Fig. 2 and subsection III-C). As shown in Fig. 4, the increased channel identification errors impose capacity losses on all four HDR versions of STAR-ISR-TR which are limited to just 2 users. The corresponding loads reduce to 10, 11, 11 and 12 simultaneous users per cell or per sector, respectively. On the other hand, the 2D-RAKE-PIC cannot operate at all with 1% pilot-symbol overhead. With 2% overhead, it can accommodate one user only. For an overhead of 20% or higher, its capacity increases and saturates at a maximum of 2 simultaneous users per cell or per sector (*i.e.*, a useful information load of 1.6). Thus, in adverse channel conditions, the performance advantage of STAR-ISR-TR over the 2D-RAKE-PIC increases up to factor 6 in capacity and 7.5 in spectrum efficiency.

In a third set of simulations, we reconsider the initial setup with a lower data-transmission-rate of 128 Kbps after channel coding (*i.e.*, $L = 32$ and $Q = 2$, see Tab. IV). In Fig. 5, the four HDR versions of STAR-ISR-TR offer about the same throughput as in Fig. 3 with transmissions rates 4 times slower, multiplying capacities by factors in the range of 3.6 to 3.8; namely 43 , 47, 48 and 53 simultaneous users per cell or per sector, respectively (*i.e.*, only 5 to 10% loss due to 4 times less averaging in Eq. (13)). On the other hand, the 2D-RAKE-PIC with a pilot-symbol overhead of 1 and 2% (or higher), respectively, multiplies its capacity by factors of 5 and 5.3 at 15 and 16 users per cell or per sector, thereby reducing the capacity gains of STAR-ISR-TR to about factor 3.3. This result suggests that the 2D-RAKE-PIC recovered from very severe performance losses due previously to challenging operation of RAKE-type receivers at a very low spreading factor (8 instead of 32). With the proposed HDR implementation, the 2D-RAKE-PIC is definitely able to operate at processing gains lower than 32. Yet, despite this improvement, results suggest that it remains much less efficient than STAR-ISR-TR with the same complexity, more so for faster HDR transmissions.

V. Conclusions

In this work we modified the STAR-ISR receiver to operate over wideband CDMA channels with delay spreads larger than the symbol duration to extend its applicability to HDR transmissions. Such low processing gain situations render symbol timing extremely difficult, especially with RAKE-type receivers. Yet the 2D-RAKE-PIC is currently accepted as the best receiver candidate for implementation. As a reference, we also developed an enhanced HDR implementation of the 2D-RAKE-PIC. For HDR links of 512 Kbps in 5 MHz bandwidth, simulation results indicate that STAR-ISR-TR outperforms the 2D-RAKE-PIC by factor 4 to 5 in spectrum efficiency while requiring the same order of complexity. The efficiency gain increases up to factor 7.5 in high Doppler. These results suggest that STAR-ISR offers a future upgrade path to greater capacities with significant performance advantages over competing receiver solutions currently envisaged for implementation with equivalent complexity.

References

[1] S. Affes, H. Hansen, and P. Mermelstein, "Interference subspace rejection: A framework for multiuser detection in wideband CDMA", *IEEE J. Selec. Areas Comm.*, vol. 20, no. 2, pp. 287-302, February 2002.

[2] K. Cheikhrouhou, S. Affes, and P. Mermelstein, "Impact of synchronization on performance of enhanced array-receivers in wideband CDMA networks", *IEEE J. Selec. Areas Comm.*, vol. 19, no. 12, pp. 2462-2476, December 2001.

[3] S. Affes and P. Mermelstein, "A new receiver structure for asynchronous CDMA: STAR - The spatio-temporal array-receiver", *IEEE J. Selec. Areas Comm.*, vol. 16, no. 8, pp. 1411-1422, October 1998.

[4] T.S. Rappaport, *Wireless Communications, Principles and Practice*, Prentice Hall, 1996.

[5] 3rd Generation Partnership Project (3GPP), Technical Specification Group (TSG), Radio Access Network (RAN), Working Group (WG4), *UE Radio Transmission and Reception (FDD)*, TS 25.101, V3.4.1, 2000.

[6] 3rd Generation Partnership Project (3GPP), Technical Specification Group (TSG), Radio Access Network (RAN), Working Group (WG4), *Base Station Conformance Testing (FDD)*, TS 25.141, V3.3.0, 2000.

[7] 3rd Generation Partnership Project, Technical Specification Group (TSG), Radio Access Networks (RAN), *Physical Layer Aspects of UTRA High Speed Downlink Packet Access*, 3GPP TR 25.848, V4.0.0, 2001.

[8] S. Affes, H. Hansen, and P. Mermelstein, "Interference subspace rejection in wideband CDMA: Modes for mixed-power operation", *Proc. of IEEE ICC'01*, 2001, vol. 2, pp. 523-529.

[9] Y.J. Guo, S. Vagdama, and Y. Tanaka, "Advanced base station technologies for UTRA", *Electronics & Communications Journal*, pp. 123-133, June 2000.

[10] K. Higuchi, A. Fujiwara, M. Sawahashi, "Multipath interference canceller for high-speed packet transmission with adaptive modulation and coding scheme in W-CDMA forward link", *IEEE J. Selec. Areas Comm.*, vol. 20, no. 2, pp. 419-432, February 2002.

[11] M. Sawahashi, K. Higuchi, and F. Adachi, "Experiments on pilot symbol-assisted coherent multistage interference canceller for DS-CDMA mobile radio", *IEEE J. Selec. Areas Comm.*, vol. 20, no. 2, pp. 433-449, February 2002.

[12] J. Chen, J. Wang, and M. Sawahashi, "MCI cancellation for multicode wideband CDMA systems", *IEEE J. Selec. Areas Comm.*, vol. 20, no. 2, pp. 450-462, February 2002.

[13] S. Affes, A. Louzi, N. Kandil, and P. Mermelstein, "A high capacity CDMA array-receiver requiring reduced pilot power", *Proc. of IEEE GLOBECOM'2000*, 2000, vol. 2, pp. 910-916.

[14] S. Affes, H. Hansen, and P. Mermelstein, "Near-far resistant single-user channel identification by interference subspace rejection in wideband CDMA", *Proc. of IEEE SPAWC'01*, 2001, pp. 54-57.